Flow Structure in a Three-Dimensional Bubble Column and Three-Phase Fluidized Bed

R. C. Chen, J. Reese, and L.-S. Fan
Dept. of Chemical Engineering, The Ohio State University, Columbus, OH 43210

Macroscopic flow structures of 3-D bubble columns and gas-liquid-solid fluidization systems under various operating conditions are studied using particle image velocimetry. Flow visualization is also conducted with the aid of a laser sheeting technique. The refractive index matching technique is used to eliminate the opaqueness of solid particles occurred in the visualization study of gas-liquid-solid fluidization. Three flow regimes (dispersed bubble, vortical-spiral flow, and turbulent flow) are identified. The flow structure is investigated for various operating variables including liquid velocity, gas velocity, and particle holdups. Four flow regions (descending flow, vortical-spiral flow, fast bubble flow, and central plume) can generally be characterized in the vortical-spiral flow regime where the gross circulation pattern occurs. A conceptual model for the flow structure in the vortical-spiral flow regime is discussed. The transition of the flow regimes and structure in the vortical-spiral flow regime is postulated to be related to the Taylor instability for flow between two concentric rotating cylinders. Similarities between the flow structures of 2- and 3-D beds are also discussed.

Introduction

Bubble columns and three-phase fluidized beds are widely used in industrial operation. Three different flow regimes, namely, dispersed bubble, coalesced bubble, and slugging, are commonly identified for bubble or slurry bubble column systems (Fan, 1989). A gross circulation flow pattern is observed for these systems under both dispersed bubble and coalesced bubble regimes (Hills, 1974; Lin et al., 1985; Latif and Richardson, 1972; Reese et al., 1992). Generally, the gross circulation flow field comprises an upward flow in the column core and a downward stream along the wall with the inversion point (zero liquid velocity) located at about 0.5 to 0.7 radius of the column (Walter and Blanch, 1983).

Most of the previous studies overwhelmingly assumed the flow field to be one-dimensional and time-invariant, although the flows are generally identified to be dynamic and multidimensions in nature (Franz et al., 1984). Hills (1974) used a modified pitot tube to measure both the mean and fluctuating velocities of the liquid circulation induced by the bubble motion; the work has been widely adopted as a data source for model verification. Latif and Richardson (1972), through the measurement of the 3-D flow information of the solids phase in a liquid fluidized bed, demonstrated that the solids phase moves in the above-mentioned gross circulation flow pattern with negligible radial circulatory motion. Recently, Devanathan et al. (1990) adopted the radioactive particle tracking technique (CARPT) to obtain the time/volume-averaged liquid flow fields in a bubble column and found the existence of one or two pairs of circulation cells depending on the gas velocity which indicates the important dependence of the flow patterns on the gas flow rate. Since the circulation structure reported by Latif and Richardson (1972) and Devanathan et al. (1990) was based on the time and modified ensemble averaged velocity profiles, this flow structure does not represent the instantaneous macroscopic flow structure in the system. The column verticality and gas distributor design may delay the onset of and may change the size of the circulation flow structure in a bubble column (Tinge and Drinkenburge, 1986; Rice and Littlefield, 1987; Rice et al., 1990, 1993); however, the gross circulation will eventually be observed.

Through the analysis of the "instantaneous" axial, tangential and radial velocity and turbulence intensity profiles measured by using hot-film anemometry (HFA), a structural flow

Correspondence concerning this article should be addressed to L.-S. Fan.

model comprising three zones was postulated by Franz et al. (1984) for the flow in a bubble column. The work is significant as it provides important experimental evidence regarding the dynamic nature of the flow structure. By using viscous and non-Newtonian liquids, Ulbrecht et al. (1985) were able to visually identify three distinct instantaneous flow patterns (viscous mode, helical flow mode, and vortex mode) in a bubble column. They concluded that the range of existence of these three flow patterns depends on the gas flow rate, the diameter of the column, and the viscosity of the liquid. Drahoš et al. (1992) investigated the instantaneous liquid flow pattern in a bubble column by using visualization (injection of methylene blue) associated with the analysis of the wall pressure fluctuations and measurements of residence time distribution of both phases. The concept of one pair of circulation cells often observed in a shallow 2-D bed was not observed in their study. They suggested a flow structure of multicell, single-loop circulation. Their analysis also supported the behavior of spiral upward flow of central macrovortex proposed by Franz et al. (1984). It is apparent that the observed instantaneous flow structures, when the gross circulation occurs, differ from the results obtained by the time/volume-averaging. There is also no clear linkage between the instantaneous flow structures and the time/volume-averaged structures.

The complex flow phenomenon in a 3-D column can be reflected in light of that in a 2-D column. Tzeng et al. (1993) studied the flow structure in a 2-D column which was reported by Reese et al. (1992) to be of great resemblance to that in a 3-D column.

Mathematical modeling of bubble-induced liquid circulation was, in most cases, conducted based on the mass and momentum balance and the assumption of the existence of one pair of symmetric circulation cells (Rietema and Ottengraf, 1970; Ueyama and Miyauchi, 1979; Clark et al., 1987; Anderson and Rice, 1989; Rice and Geary, 1990; Geary and Rice, 1992). While the predicted axial velocity profile compared fairly well with Hills' (1974) data, the adoption of isotropic turbulence concept and the empirical laminar or turbulence equation for single-phase flow conflicts with the experimental results (Franz et al., 1984) of which the turbulence structure is oriented by the bubble rising patterns. The modeling work usually requires the input of an empirical gas holdup profile. It should be noted, however, that the circulation pattern is significantly affected by the gas holdup profile as demonstrated by Clark et al. (1987).

Based on the energy balance, a modified model was developed by Joshi and Sharma (1979) following the work of Whalley and Davidson (1974). Instead of one pair of circulation cells, a circulation structure of multiple stationary cells is proposed (Joshi and Sharma, 1979; Joshi, 1980). The underlying assumption of the structure of the multiple circulation cells in the axial direction in their work, as well as the flow structure of multiple circulation cells in the transverse direction assumed by Bhavaraju et al. (1978), remains to be experimentally clarified.

Despite extensive theoretical and experimental efforts in unveiling the flow mechanism of the circulation flow field, more studies leading to better understanding and ultimate prediction of the flow structures of bubble columns and three-phase fluidized beds are necessary. Specifically, the instantaneous, rather than average, circulation structure in these systems needs to be further explored. In this study, experiments are conducted in a 10.2 cm ID column to explore the dynamic (instantaneous) macroscopic flow structure of both bubble columns and three-phase fluidization systems. The laser sheeting technique for a full-field measurement, coupled with particle image velocimetry (PIV), is utilized for visualization and quantification of the flow structures. A conceptual model of the flow structure is postulated based on the observations. The effects of gas and liquid flow rates on the macroscopic flow behavior are studied.

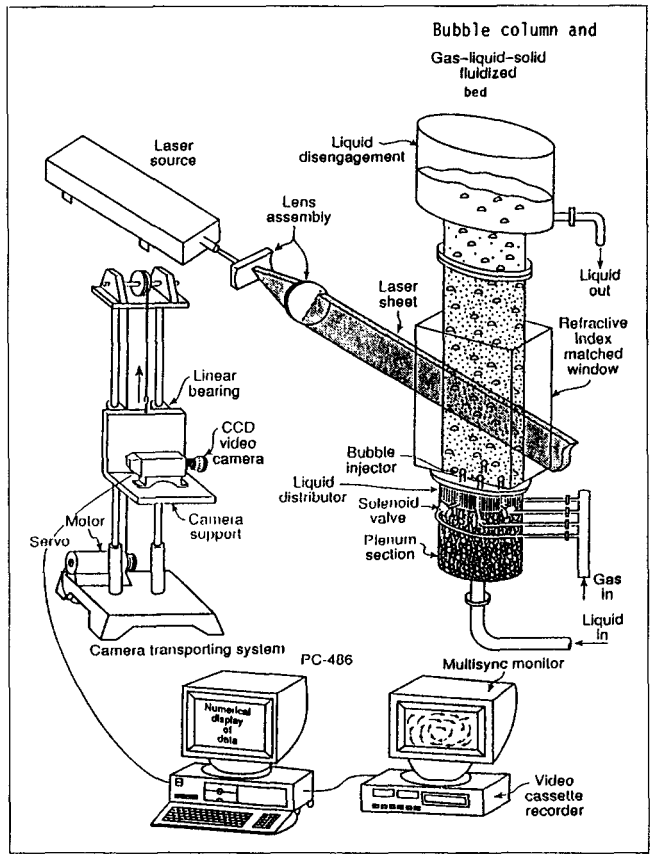

Figure 1. Experimental apparatus and PIV system.

Experimental Studies

Figure 1 shows the experimental apparatus. The entire column including the distributor section and the disengagement section is 2.2 m high and is made of plexiglas except the visualization section which is made of 10.2 cm ID and 1.2 m high Pyrex glass. The refractive index matching technique is applied to minimize the tube curvature effect which not only decreases the extent of image receivable by the video camera but also causes difficulty in the ascertainment of the laser sheet location. This is conducted by enclosing the test section in a rectangular box with a glass window whose refractive index is the same as that of the glass tube and filling the box with a fluid (sodium iodide solution 55 wt. %) of the same refractive index (≈ 1.474) as that of glass. The technique is also used to circumvent the light blockage problem caused by opaque particles. The sodium iodide solution of 55 wt. % matched the refractive index of glass beads. Care should be exercised, however, in interpreting the experimental results obtained using the refractive index

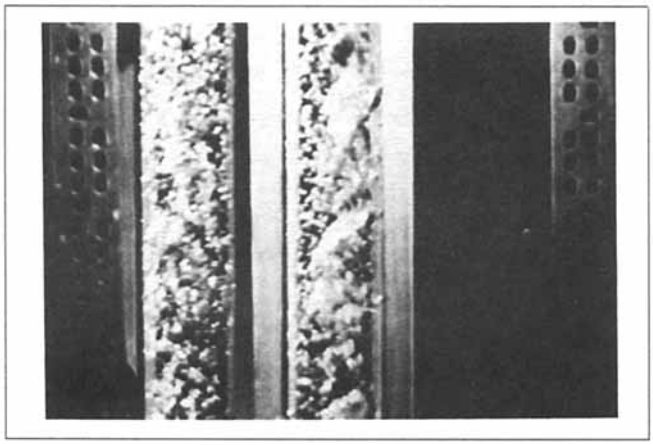

Figure 2. Flow pattern of the central bubble stream in a gas-liquid bubble column system.

$U_g = 2.9$ cm/s and $U_l = 0$ cm/s.

matching fluid as it may alter the hydrodynamic characteristics of the system through the change of liquid properties.

A tube-orifice type of distributor (Fan et al., 1982) is used to provide uniformity of gas and liquid flows. Tap water is used as the liquid phase for most cases. The sodium iodide solution, however, is used for the test of three-phase fluidization when the refractive index matching technique is applied. Neutrally buoyant Pliolite particles of 200–500 μm are used as the liquid tracer. To ensure that the seeding particles follow the flow closely and have virtually no effects on the flow behavior, the concentration of the seeding particles is maintained below 0.1% and the Stokes number of the seeding particles is ascertained to be much smaller than 1. Air is used as the gas phase. The gas pressure is maintained within 4 to 10 psig (28 to 69 kPa) upstream of the gas plenum. The superficial gas velocity ranged from 0.1 to 5.5 cm/s, and the superficial liquid velocity ranged from 0.0 to 7.4 cm/s in this study. Two types of particles including 500 μm glass beads ($\rho_s = 2.5$ g/cm^3) and 1.5 mm acetate beads ($\rho_s = 1.25$ g/cm^3) are used as the solids phase. The solids holdup ranged from 0 to 10% in this study.

The laser sheeting technique is utilized for flow visualization. A 4 W argon ion laser system is used as the laser source, and a laser sheet of 2–5 mm thickness is created through the use of a cylindrical lens. Measurements are conducted at several different radial locations with the laser sheet projected along the vertical axial plane. A high resolution (800×490 pixel) CCD camera equipped with variable electronic shutter ranging from 1/60 to 1/8,000 s is utilized to record the image of the flow field. A slide mirror oriented at an angle of 45° to the front view of the column is used to observe the flow at the location 90° from the front; images of both the front and side views are recorded simultaneously in a same video frame (Figure 2). The 3-D motion of the central bubble stream is then identified by correlating the bubble motion from both images.

A particle image velocimetry (PIV) system developed by Chen and Fan (1992) is applied to measure local flow properties of a 3-D fluidized bed. This PIV technique consists of laser sheeting, video recording, and image processing as the three major parts. Besides the ability of measuring the full-field flow information including velocity vectors, holdups, and accelerations, this PIV system is able to discriminate the flow properties among different phases which renders it unique and suitable for three-phase fluidization measurements. A complete description of the operating principles and calibration of the PIV system can be found in Chen and Fan (1992). Note that all the gas or liquid velocities described in this article refer to the superficial velocities unless otherwise noted.

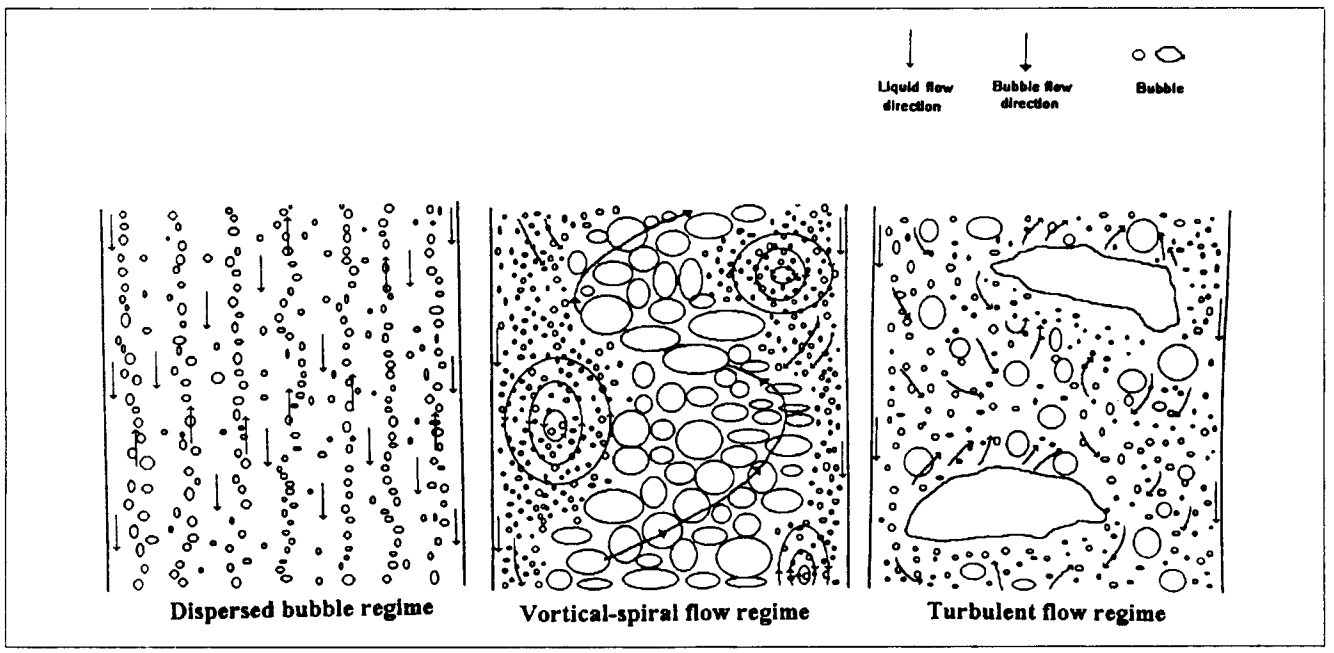

Figure 3. Flow regimes in a 3-D bubble column and gas-liquid-solid fluidization system.

Results and Discussion

Macroscopic flow structures

Flow visualization is first conducted for the flow in a bubble column. Figure 3 summarizes the three different flow regimes which can be identified in a bubble column: the dispersed bubble, vortical-spiral flow and turbulent flow regimes. When compared with the regime classification reported earlier (for example, Deckwer et al., 1980), it is apparent that the coalesced bubble (churn-turbulent) flow regime commonly referred to in the literature can be subdivided further into two flow regimes—vortical-spiral flow and turbulent flow, based on inherently different flow mechanism and flow structure observed in this study. The demarcation criteria of the flow regimes may vary with design or operating variables such as column size, type of distributor, and liquid properties. Macroscopic flow structures in the three flow regimes, with an emphasis on the vortical-spiral flow regime, are discussed below. The results are based on the observation of the in-bed zone (or bulk fluidized bed zone, Fan, 1989) in the column, and further study is required for the inlet zone (or gas-liquid distributor zone) and disengagement zone (or freeboard zone) of a 3-D column. The results are based on a liquid-batch system unless otherwise noted.

Dispersed bubble flow regime

At a low gas velocity, the bubble streams are observed to rise rectilinearly with relatively uniform size distribution along the column radius. Bubble coalescence is insignificant in this dispersed bubble regime. The liquid is carried up by the bubble-driven motion in the vicinity of the ascending bubble streams and falls downward between these bubble streams. A typical liquid flow pattern in the dispersed bubble regime in Figure 4 is for the liquid flow field at the plane of 0.75 radius (of the column) with a gas velocity of 1 cm/s. While the liquid falls straight downward shown at the top part of the figure, the ascending bubbles (located outside this photo) cause the downward liquid motion to move in a chaotic manner as shown at the bottom part of Figure 4. Dynamic vortices may be observed occasionally as the bubbles pass through the laser sheet. However, straight downward liquid flow motion is the flow pattern most often observed in the dispersed bubble regime which exists for a gas flow rate up to about 1.7 cm/s.

Vortical-spiral flow regime

With a further increase in the gas velocity, the migration motion of the bubbles becomes intensified even at the region immediately above the gas distributor. For the gas velocity between 1.7 and 2.1 cm/s, the bubbles mainly move in clusters with no bubble coalescence observed. Due to the migration motion, however, the bubbles start forming the central bubble stream which moves in a rocking spiral manner. The bubble coalescence and breakup become evident as the gas velocity reaches about 2.1 cm/s. In the meantime, the rotating frequency of the central bubble stream is intensified as the gas velocity increases and results in a more clearly observable spiral motion of the central bubble stream. Figure 2 represents the spiral flow pattern of the central bubble stream for a gas velocity of 2.9 cm/s. It is interesting to note that although the formation of clusters of bubbles is diminished with the increase

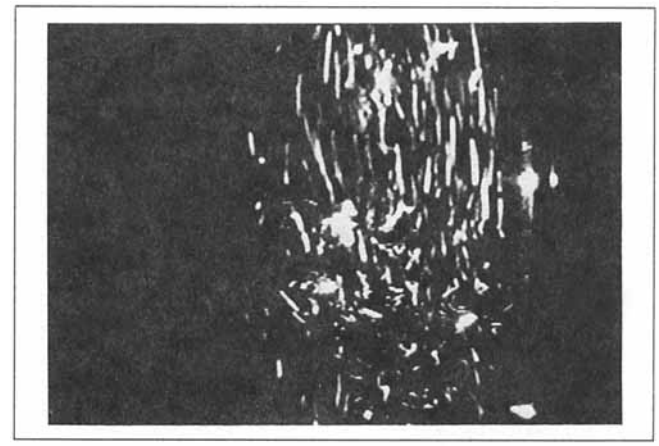

Figure 4. Liquid flow field at the plane of 0.75 radius in a gas-liquid bubble column system.

$U_g = 1.0$ cm/s and $U_l = 0$ cm/s.

of the gas velocity, the clusters do not completely disappear until the gas velocity increases up to about 4.9 cm/s. Thus, in the gas velocity range of 2.1 to 4.9 cm/s, the central bubble stream which consists of coalesced bubbles and bubble clusters not only spirals upward but also swings laterally back and forth. In the region between the central bubble stream and the column wall, tiny bubbles are observed to move up and down which also indicates the dynamic nature of this region. The liquid phase is carried upward by the spiral motion of the central bubble stream and flows downward in the same spiral manner between the central bubble stream and column wall. The liquid flowing downward in this spiral manner also demonstrates a vortical flow pattern with the vortices appearing in the longitudinal direction relative to the vertical column axis. These vortices, however, may lay in the transverse direction relative to the downward liquid stream. Figure 5 clearly shows the liquid flow field of a bubble column, at the plane of 0.75 radius for a gas velocity of 3.3 cm/s, as a diagonal downward liquid flow (from upper-right corner to the lower-

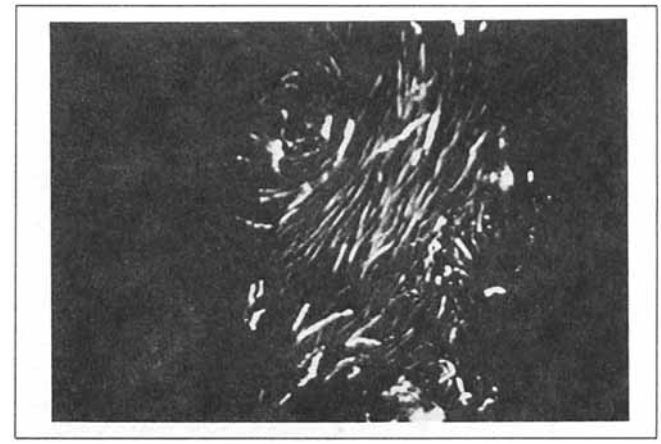

Figure 5. Liquid flow field at the plane of 0.75 radius in a gas-liquid bubble column system.

$U_g = 3.3$ cm/s and $U_l = 0$ cm/s.

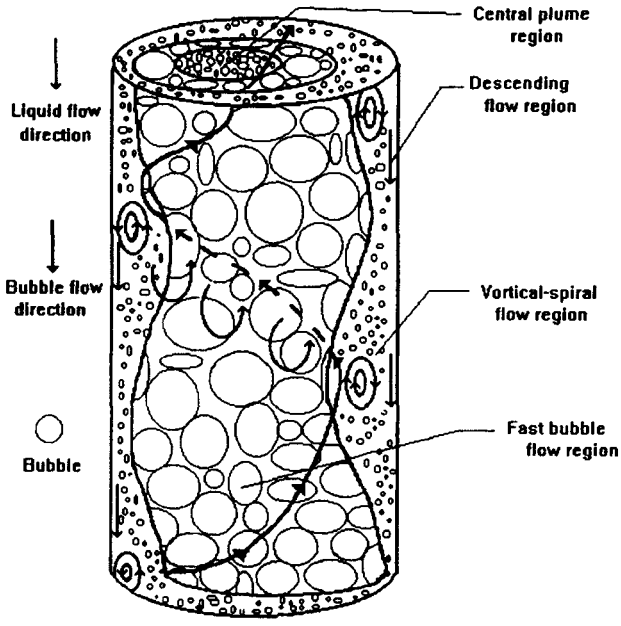

Figure 6. Flow structure in the vortical-spiral flow regime in a 3-D gas-liquid bubble column and gas-liquid-solid fluidization system.

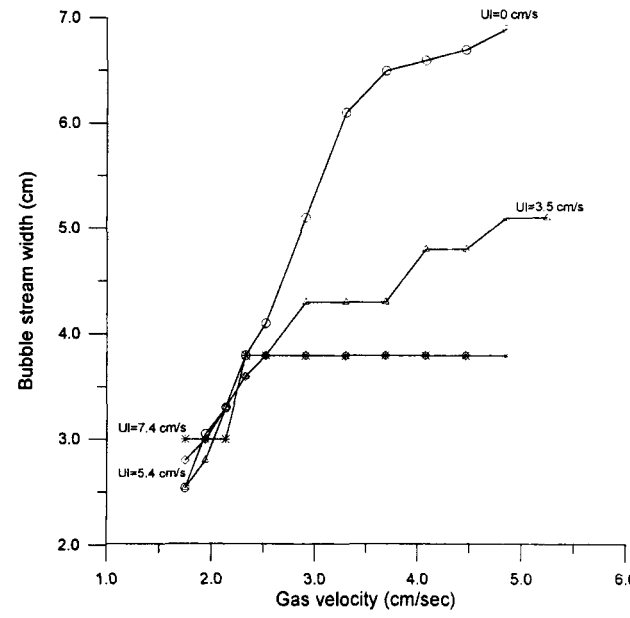

Figure 7. Variation of the width of central bubble stream with gas and liquid velocities in a gas-liquid bubble column system.

left corner) with vortical motion (on the upper-left, corner). Since the thickness of the laser sheet is small but finite, it allows for the observation of "local" 3-D liquid flow motion. The 3-D spiral and vortical liquid flow patterns are identified through the observation of the flow field in the laser sheet projected at several different radial locations. Actually, this 3-D vortical-spiral liquid motion is identified much more easily with a VCR when playing in slow motion (Reese et al., 1992). Therefore, in this vortical-spiral flow regime (for gas velocity from 2.1 to 4.2 cm/s), the liquid phase is carried up by the central bubble stream which spirals upward in the column center and falls down in a vortical and spiral pattern in the region between the central bubble stream and the column wall.

Based on the observation described above and the general flow structure of a large 2-D column (column width, 48.3 cm) observed in Tzeng et al. (1993), the general macroscopic flow structure of a 3-D column in the vortical-spiral flow regime is proposed in Figure 6, together with the four flow regions—descending flow region, vortical-spiral flow region, fast bubble flow region, and central plume region. The descending flow region, located adjacent to the column wall, is characterized by downward liquid and/or solids streams moving in either straight or spiral manner depending on the gas and liquid velocities. This region is free of bubbles at low gas velocities. At relatively high gas velocities, however, tiny bubbles can be observed in this region. The size of this region will change with the gas velocity.

The vortical-spiral flow region, located between the descending flow region and the central bubble stream, is characterized by the existence of spiral-downward liquid and/or solids vortices. The spiral-descending velocity varies with gas and liquid velocities. The entire region is swinging laterally back and forth closely related to the swinging motion of the neighboring fast bubble flow region. Vortices are rather dynamic due to disturbances caused by small bubbles trapped in this region and by large bubbles rising in the fast bubble flow region. Good interphase mixing characteristics can be found in this region.

Adjacent to the vortical-spiral flow region is the fast bubble flow region, also referred to herein as the central bubble stream, where significant bubble coalescence and breakup take place. In this region, clusters of bubbles or coalesced bubbles move upward in a spiral manner with high velocity. There could be more than one spiral bubble stream simultaneously existing and the spiral direction will change dynamically. These spiral bubble streams swing laterally back and forth over almost the entire bed diameter at high gas velocities. This region also serves as a baffle on the radial mass transfer for both solids and liquid phases between the central plume region and the vortical-spiral flow region. When the vortical-spiral flow regime is established, the fast bubble flow region dictates the macroscopic flow structure of the system.

The central plume region is located in the column core and is surrounded by the fast bubble flow region. This region is characterized by a relatively uniform bubble size distribution and less bubble-bubble interaction. Note that the central plume region is indistinguishable in the 10.2 cm ID column employed in this study due to the mergence with the fast bubble flow region; however, it is expected to be seen in the flow structure of a large column. Further research on these scale-up effects is necessary.

The relationship between the width of the central bubble stream and the gas velocity is demonstrated in Figure 7. The width of the central bubble stream increases linearly (to about 6.7 cm) with the increase of gas velocity from 1.8 up to about 3.8 cm/s. As the gas velocity increases over 3.8 cm/s, the width of the central bubble stream remains constant at about 6.7 cm regardless of the increase in gas velocity. Spiral motion of the central bubble stream is visually identified for the gas velocity between 2.1 and 4.2 cm/s, which is comparable to the range of gas velocity for the linear increase of central bubble stream

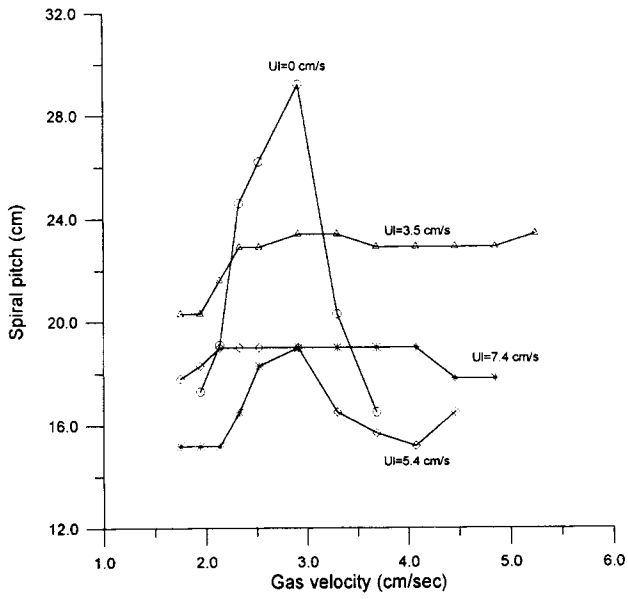

Figure 8. Variation of the pitch of the spiral motion of central bubble stream with gas and liquid velocities in a gas-liquid bubble column system.

width as shown in Figure 7. Therefore, the results of Figure 7 can also contribute to the determination of the flow regime demarcation from vortical-spiral flow to turbulent flow (as will be discussed later). Note that the maximum width of the central bubble stream (6.7 cm) is of the same order as the large coalesced bubbles in the turbulent flow regime. The pitch of the spiral motion of the central bubble stream is closely related to the gas velocity in Figure 8. The pitch of the spiral motion first increases nearly linearly with the increase of the gas velocity until it reaches a maximum value (30 cm at $U_g = 3$ cm/s) and then decreases in a linear way with the increase in gas velocity until the spiral motion becomes indistinguishable.

The effects of liquid velocity on the flow structure in the vortical-spiral flow region shown in Figures 7 and 8 present the relationship of gas and liquid velocities with the width and pitch of the spiral motion of the central bubble stream, respectively. The increase of liquid velocity retards the bubble coalescence and results in a decrease in the width of the central bubble stream. The sizes of bubbles are observed to be significantly decreased with an increase in liquid velocity. The forced upward flow of the liquid also regulates the flow pattern of the rising bubbles. This forced liquid flow results in a flow structure with less bubble-bubble interactions and a smaller size of the central bubble stream. In the case of the liquid velocity of 7.4 cm/s, swarms of bubbles instead of coalesced bubbles are found in the central bubble stream under the vortical-spiral flow regime. The bubbles do not coalesce until the transition regime is reached between the vortical-spiral flow and the turbulent flow regimes. For both cases of liquid velocity of 5.4 and 7.4 cm/s, the width of the central bubble stream is reduced to about one-half of that under the liquid-batch condition and remains constant over a wide range of gas velocities.

The spiral motion of the central bubble stream is also affected by the increase in liquid velocity as shown in Figure 8. The increase of liquid velocity decreases the spiral pitch especially for gas velocity below 3.0 cm/s. Further increase of gas velocity results in two different observations. For the cases of liquid-batch and liquid velocity of 5.4 cm/s, the spiral pitch decreases with the increase of gas velocity. For the other two cases of liquid velocity of 3.5 and 7.4 cm/s, the spiral pitch remains nearly constant with the increase in gas velocity. However, it is interesting to note that the maximum value of spiral pitch for all cases occurs at the gas velocity of about 3.0 cm/s. The decrease in spiral pitch with an increase in gas velocity can be related to the formation of clusters of bubbles or coalesced bubbles. The spiral energy of the central bubble stream increases with the formation of large bubbles due to the bubble coalescence or clustering of bubbles. The increase in spiral energy results in the retainment or decrease of the spiral pitch. The spiral motion is gradually destroyed as the sizes of coalesced bubbles become significant of which the bubble wake and drift effects caused by bubble motion dominate.

Analysis

Centrifugal instabilities may play an important role in determining the macroscopic and microscopic flow phenomena in the system. Specifically, it is likely that these flow phenomena are attributed to a combination of the Taylor-Couette instability, the Dean instability, and the Taylor-Goertler instability (Drazin and Reid, 1981; Fiebig and Mitra, 1993). The Taylor-Couette instability, however, is most closely associated with the formation of the macroscopic flow structure in the vortical-spiral flow regime. As mentioned above, in the vortical-spiral flow regime, the fast bubble flow region not only moves up in a spiral manner but also isolates the central plume region from direct mass exchange with the vortical-spiral flow region. Therefore, the bubble streams in the fast bubble flow region essentially act as a rotating "solid" boundary with axial motion. Neglecting the laterally swinging motion of the fast bubble flow region, the flow can be simulated as that between two concentric (or slight eccentric) rotating cylinders of which the inner-cylinder (the fast bubble flow region) is in motion and the outer-cylinder (column wall) is at rest. The motion of inner cylinder consists of rotation and axial displacement.

The flow between concentric rotating cylinders has attracted numerous studies since the earliest work conducted by Couette (1890). The stability of the flow of a viscous liquid between concentric rotating cylinders was first studied, both experimentally and theoretically, by Taylor (1923) who described that flow vortices (Taylor vortices) appear when a certain Reynolds number has been exceeded. These Taylor vortices completely fill the annulus between the two cylinders and rotate in alternately opposite directions. He attributed this flow phenomenon to instability of flow transition from laminar to turbulent and introduced a characteristic number known as Taylor number, T_a, of the following form to express the instability criterion:

$$T_a = \frac{U_i(b-a)}{\nu}\sqrt{\frac{(b-a)}{b}} \tag{1}$$

In Eq. 1, U_i is the peripheral velocity of the inner cylinder; ν is the kinematic viscosity of liquid; and a and b are the inner-

and outer-cylinder radii. A laminar flow with Taylor vortices was suggested in the range of the Taylor number between 41.3 and 400. If U_i can be assumed to equal the product of Ω_i (angular velocity of the fast bubble flow region) and a (radius of the fast bubble flow region), the above criterion range of Taylor number corresponds to an angular velocity range of 0.2 to 1.2 rad/s for the fast bubble flow region in this bubble column. The observed angular velocity of the fast bubble flow region in this study is about 6 rad/s, which is clearly beyond the range suggested by Taylor (1923). It signifies that the vortical flow structure in the vortical-spiral flow region may not be a laminar flow with Taylor vortices. Recently, a thorough study of the flow states between two concentric rotating cylinders was conducted by Andereck et al. (1986). A surprisingly large variety of different flow regimes (as many as 26), which are characterized by the parameters such as the radius ratio, the aspect ratio, the inner- and outer-cylinder Reynolds numbers, and the end conditions, are revealed in their work. They provide flow-regime diagrams for different inner- and outer-cylinder Reynolds numbers under constant radius ratio (0.883) and aspect ratio (30). The inner- and outer-cylinder Reynolds numbers are defined as:

$$R_i = \frac{a(b-a)\Omega_i}{\nu} \tag{2}$$

and

$$R_o = \frac{b(b-a)\Omega_o}{\nu} \tag{3}$$

Considering the flow-regime diagrams given by Andereck et al. (1986), a Taylor-vortex flow state exists for R_i between 120 and 160 for the outer-cylinder at rest. This again corresponds to a very low angular velocity ($\Omega_i < 1$ rad/s) of the fast bubble flow region in the present column system which is lower than the angular velocity of the fast bubble flow region observed in this study. Increasing the rotating speed of the inner cylinder leads to the turbulent Taylor vortices regime which starts from $R_i = 1{,}370$ for $R_o = 0$ (Andereck et al., 1986). This turbulent Taylor vortices regime corresponds to an angular velocity of the fast bubble flow region of 2.4 rad/s and up in the present column system. It therefore appears that the vortical flow structure in the vortical-spiral flow regime is analogous to the turbulent Taylor vortices structure.

Besides the Taylor vortices form of instability, a vortical-spiral instability form was also observed by Taylor (1923) in the flow between two concentric rotating cylinders. Taylor (1923) reported that the formation of a spiral instability always appears after an axial circulation occurs. By analogy, the spiral motion of the liquid flow in the vortical-spiral flow region is due to the axial motion of the fast bubble flow region. This is confirmed by Ludwieg (1964) who conducted experiments to investigate the stability of the flow between two concentric rotating cylinders by including the case when the two cylinders are axially displaced relative to each other. An unstable flow with vortices in the shape of spirals is observed. By considering the axially asymmetric disturbances, he also derived a stability criterion for an inviscid and incompressible fluid flow. Ludwieg's (1964) work clearly indicates that the effects of the imposed axial motion on the inner cylinder results in a "twist" of the Taylor vortices and then the final product of spiral Taylor vortices. This is indeed similar to the flow structure in the vortical-spiral flow region caused by the movement of the fast bubble flow region which is not only rotating but also axially rising up. The determination of the prevailing flow regimes for an annulus with a given uniform axial stream was derived by Kaye and Elgar (1958) based on their own experimental data. This criterion is determined by three characteristic numbers: the Taylor number T_a, a Reynolds number Re_d formed with the axial velocity and the width between two concentric cylinders, and the ratio between the width of the annulus and the inner-cylinder radius. A theoretical explanation of these boundaries for different flow regimes, however, is still not available (Schlichting, 1979). Nevertheless, according to Kaye and Elgar's (1958) criterion ($T_a > 150$), the flow in the vortical-spiral flow region in this test is located in the region of turbulent flow with vortices. It should be noted that the fast bubble flow region is observed to be of spiral shape which differs from the experiment conducted by using rotating solid cylinder imposed with axial motion (Kaye and Elgar, 1958; Ludwieg, 1964). Apparently, the literature concerning the flow structures between two concentric rotating cylinder with the inner cylinder of spiral shape is lacking. The effects of the spiral shape of the fast bubble flow region on the flow structure of the vortical-spiral flow region are therefore not clear presently. The vortices observed in the vortical-spiral flow region may also be attributed to Dean's instability if the vortices do indeed lie in the transverse plane with respect to the flow direction.

The above-mentioned instability form of the flow between two concentric rotating cylinders is essentially similar to that observed for the flow structure in the vortical-spiral flow regime except that the vortical-spiral flow phenomena in a 3-D column are much more dynamic in nature and complicated due to the swinging motion of the fast bubble flow region and the dynamic nature of the bubble motion. One could state that the vortical-spiral flow regime in a 3-D column basically is an unstable transition flow regime between the dispersed bubble and turbulent flow regimes. However, the application of theoretical works developed for flow between two concentric rotating cylinders to the flow in a 3-D bubble column or three-phase fluidized bed is limited. This is due to the simplified assumptions such as inviscid fluid and uniform axial velocity distribution being far from reality, and the additional effects caused by the spiral and swinging motion of the fast bubble flow region. More studies are indeed needed to quantify the effect of such instabilities of this complex flow phenomena in the vortical-spiral flow regime.

Turbulent flow regime

For the gas velocity range between 4.2 and 4.9 cm/s, large bubbles start forming and moving in a sort of "discrete" manner. As the gas velocity exceeds 4.9 cm/s, the flow pattern with discrete large bubbles separated by a certain distance can always be found. This formation of large bubbles caused by intensive bubble coalescence gradually breaks down the "continuous" structure and eventually the spiral flow pattern of the central bubble stream. Momentum is transferred from the primary bubble wakes to the surrounding liquid through the

roll-up and shedding phenomena of bubble wakes (Fan and Tsuchiya, 1990) and thus the flow structure of the bubble column is determined. Figure 9 displays the liquid flow field at the plane of 0.75 radius in a bubble column for gas velocity of 5.3 cm/s under the liquid-batch condition. A single large bubble is shown and the upward liquid flow induced primarily by bubble wake carriage (Tang and Fan, 1989) and drift induced by bubble rise (Tsuchiya et al., 1992) is evident in this figure. In this turbulent flow regime (for gas velocity over 4.9 cm/s), liquid is induced and transported by the above-mentioned bubble wake mechanism and the liquid flow pattern is much more chaotic and dynamic than that in the vortical-spiral flow regime. The liquid mixing between the bottom and the top of the column in the turbulent flow regime is not as rapid as that in the vortical-spiral flow regime.

The liquid velocity also affects the transition of the flow regimes. There is no significant evidence to show the effects of liquid velocity on the transition of the dispersed bubble regime to the vortical-spiral flow regime. However, compared with the liquid-batch condition, the increase of liquid velocity inhibits the development of the vortical-spiral flow regime into the turbulent flow regime. For the liquid velocity of 7.4 cm/s, the vortical-spiral flow structure is still clearly observed even when the gas velocity is up to 5.3 cm/s at which the turbulent flow regime prevails under the liquid-batch condition.

Comparison of 2-D and 3-D columns

Similarities have been found between the flow structures of 2-D and 3-D columns when compared with the 2-D results reported by Tzeng et al. (1993). Three flow regimes which are dispersed bubble, vortical flow (2-D) or vortical-spiral flow (3-D), and turbulent flow regimes can be identified. Four distinct flow regions, namely, descending flow region, vortical flow region (2-D) or vortical-spiral flow region (3-D), fast bubble flow region and central plume region are distinguished in the vortical flow regime (2-D) or the vortical-spiral flow regime (3-D). For both 2-D and 3-D columns, a thin layer of bubble-free descending flow is detected in the region adjacent to the (side) walls. The liquid and/or solids flow in a vortical pattern (2-D) or in a vortical-spiral pattern (3-D) in the region adjacent to the descending flow region. In the fast bubble flow region, large coalesced bubbles move with higher velocity in a wavelike motion in the 2-D column and follow a spiral motion in the 3-D column. A baffle effect of the fast bubble flow region on the radial mass transfer for both the solids and liquid phases is observed for both 2-D and 3-D columns. The central plume region existing in the column core is characterized by relatively insignificant bubble-bubble coalescence and uniform bubble size distribution. The above comparison is based on the observed results of a 48.3 cm wide 2-D column and a 10.2 cm ID 3-D column and its corresponding structures for a general 3-D structure in a large vessel in Figure 6. It is important to note that the upper and lower bounds of the flow regimes and the flow structure itself will be affected by the column design such as column size and type of gas distributor for both 2-D and 3-D column systems (Reese et al., 1992).

Particle Image Velocimetry Results

The PIV (particle image velocimetry) system is capable of providing the instantaneous, quantitative results on a flow plane including instantaneous velocity distribution of different phases, accelerations, gas and solid holdups, bubble sizes and their distributions, and other statistical flow information. The PIV system consists of schemes which identify the particle images, discriminate the particle images between phases, and compute the displacement between the particle images from successive frames. A complete description of the operating principles of the PIV system can be found in Chen and Fan (1992). The PIV results discussed below are taken at a height of 61 cm above the inlet gas distributor.

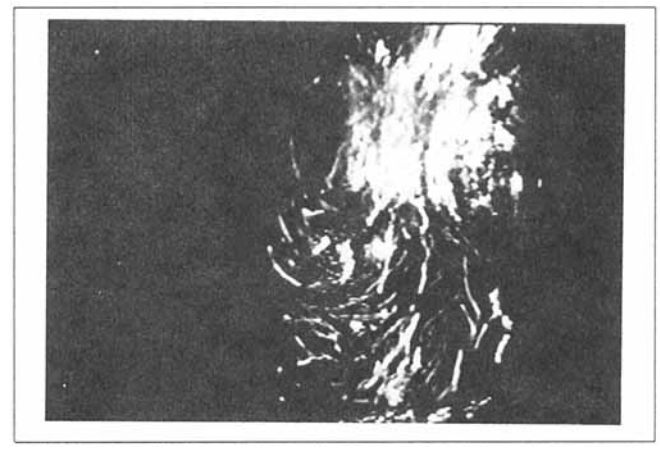

Figure 9. Liquid flow field at the plane of 0.75 radius in a gas-liquid bubble column system.

$U_g = 5.3$ cm/s and $U_l = 0$ cm/s.

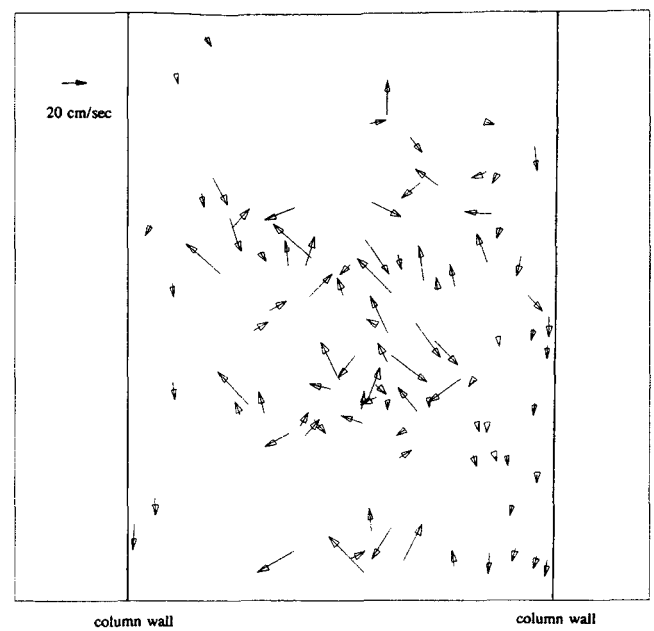

Figure 10. Instantaneous velocity vectors of liquid at the central plane in a gas-liquid bubble column system.

$U_g = 0.6$ cm/s and $U_l = 0$ cm/s.

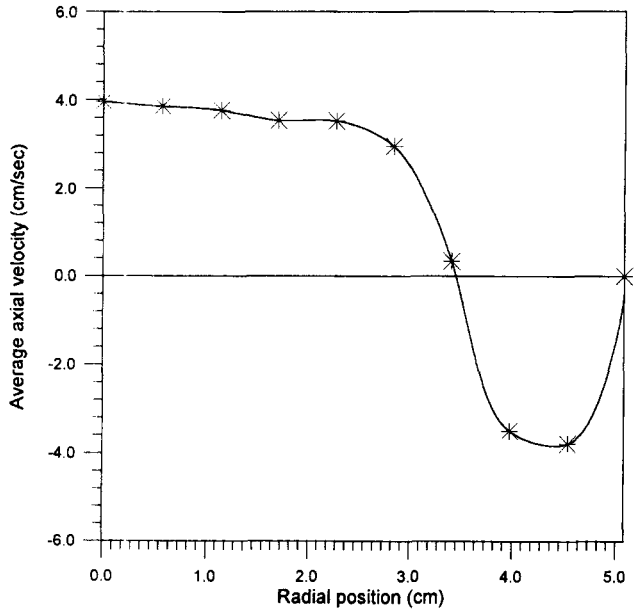

Figure 11. Average velocity profile of liquid along the radial distance in a gas-liquid bubble column system.

$U_g = 0.6$ cm/s and $U_l = 0$ cm/s.

Figure 10 shows the instantaneous velocity vectors of the liquid phase at the central plane in a 3-D bubble column for a gas velocity of 0.6 cm/s. In the region close to the wall, a thin layer of liquid flowing straight downward is clearly seen. The size of this descending flow region is about 1.1 cm and the average interstitial liquid velocity in this thin layer is about 11 cm/s. More chaotic liquid motion with higher velocity is observed in the column core. The maximum interstitial velocity can be as high as 40 cm/s. The combined effects of bubble wake and liquid drift caused by bubble motion result in the flow pattern in this column core region. No apparent vortical and spiral liquid flow can be detected under this operation condition. The same seeding particles can be found to exist in the laser plane for as long as 0.5 s. This result implies the relative insignificance of the tangential motion and therefore indirectly demonstrates the rectilinear motion of the liquid phase at low gas velocities.

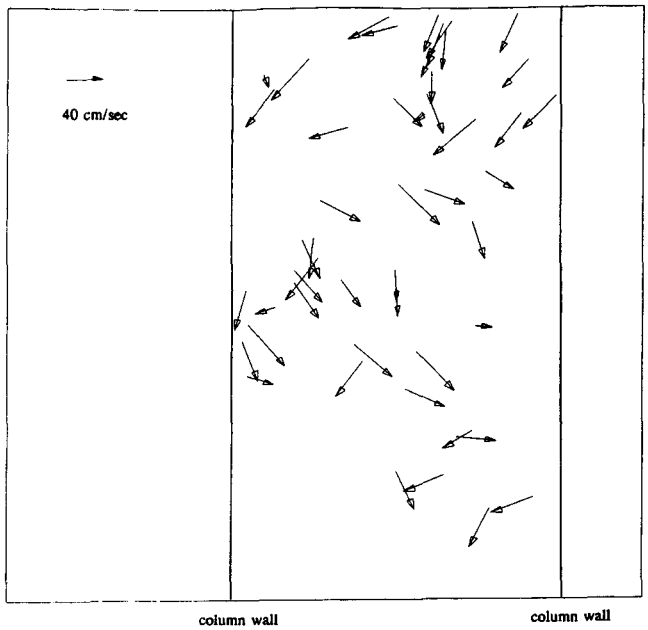

Figure 12. Instantaneous velocity vectors of liquid at the plane of 0.75 radius in a gas-liquid bubble column system.

$U_g = 2.9$ cm/s and $U_l = 0$ cm/s.

Figure 11 shows the typical time/volume average velocity profile along the radial distance for low gas velocity. The axial velocity profile is a time- and volume-averaged result from the data at more than 30 different axial locations for over 3 min at a time span of 10 s. Initially, the upward velocity decreases slowly with the radial distance to the radial location at about one half of the radius. The upward velocity than decreases sharply with the radial distance and becomes zero at the radial location of around 0.7 radius. Starting from this flow inversion point, the downward velocity increases with the radial distance to the location of 0.9 radius. This maximum downward velocity has the same value as the upward velocity at the column center. The results of Figure 11 are very similar to the results of previous studies (such as Hills, 1974). An integration of the velocity profile over the radial distance shows the conservation of liquid mass which indirectly validates the accuracy of the data. A gross circulation flow pattern with upward flow in the column core and downward flow in the column wall obtained from the present time/volume averaged axial velocity profile indicates that, on the average, a pair of liquid circulation cells exist in the bulk fluidized bed zone which is consistent with that reported in the literature (such as Hills, 1974). However, the flow visualization and the PIV results show that the liquid rises upward with the uniformly distributed rising bubbles and flows downward between these bubbles streams in this dispersed bubble regime. In the region close to the column wall, a descending liquid flow can always be found due to the lack of bubble motion. The time/volume averaged upward liquid velocity in the column core is due to the zig-zag motion of the bubbles and the larger upward liquid velocity in the vicinity of bubbles than the downward liquid flow between bubble streams. It is apparent that the postulated flow structure based on the time-average results is far from the real instantaneous flow phenomena. Some of the inherent flow mechanisms are hidden through the averaging process.

The typical example of the liquid spiral motion in the vortical-spiral flow regime in Figure 12 shows the liquid flow field in the laser sheet located at 0.75 radius. The liquid first flows diagonally downward toward the lower-left corner and turns toward the lower-right corner (at the middle of the figure) and finally turns back again toward the lower-left corner (at the bottom of the figure). Considering the finite thickness of the laser sheet, Figure 12 provides the 2-D projection of the 3-D flow field. Coupled with the results from the flow visualization, Figure 12 clearly shows the 3-D spiral motion of the liquid in the vortical-spiral flow region under the vortical-spiral flow regime. Vortices are relatively difficult to be detected by using PIV due to the dynamic nature of the vortical motion and the small thickness of the laser sheet. Only when the vortices are located on the laser sheet plane can they be observed. The flow structures in the four flow regions of the vortical-spiral flow

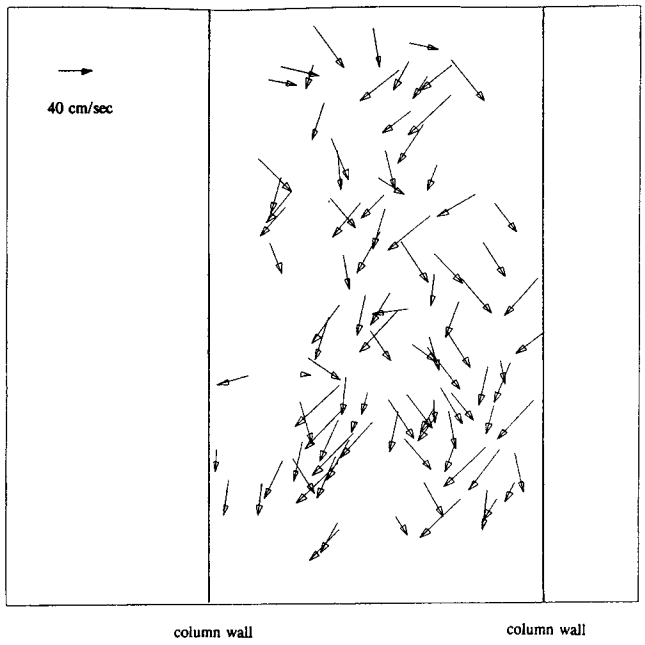

Figure 13. Instantaneous velocity vectors of liquid at the plane of 0.85 radius in a gas-liquid bubble column system.

$U_g = 4.9$ cm/s and $U_l = 0$ cm/s.

regime are instantaneous phenomena which may be overlooked when averaging procedures are used to quantify the flow properties.

The spiral, but chaotic, liquid flow pattern in the turbulent flow regime in Figure 13 shows the liquid flow field in the plane located at 0.85 radius for gas velocity of 4.9 cm/s. Since the above-mentioned characteristics (in the section of Macroscopic Flow Structures) of the bubble motion are dominant in this regime, the interaction between the bubbles and the liquid becomes significant and results in the breakup of the spiral flow pattern. As shown in Figure 13, the liquid phase still maintains the spiral manner despite the local discontinuity caused by the interaction with bubbles. When the gas velocity is further increased, the local breakup of the spiral motion becomes more significant and eventually breaks down the global central bubble stream spiral flow pattern. A slugging flow will then be experienced in a small diameter column but a fully turbulent flow will occur in a large one. Again, under the same seeding concentration, more seeding particles can be detected in Figure 13 than in Figure 12 which indirectly shows the relative insignificance of the tangential motion in the turbulent flow regime.

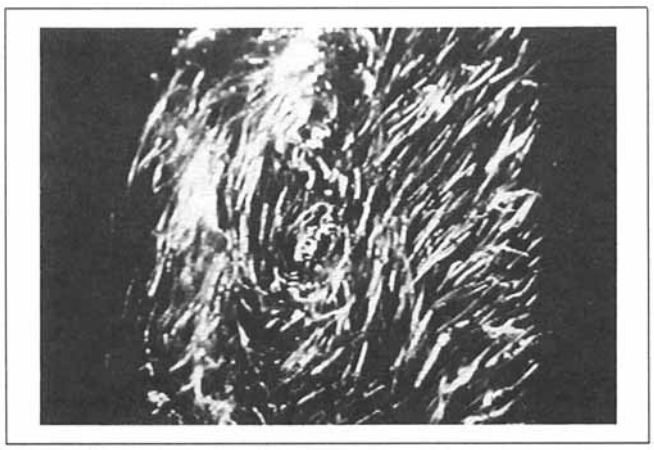

Figure 14. Liquid flow field at the plane of 0.75 radius in a gas-liquid-solid fluidization system containing sodium iodide solution and 500 micron glass beads.

$U_g = 2.9$ cm/s, $U_l = 0$ cm/s, and $\epsilon_s = 5\%$.

Particles Effects

Under the operating conditions of this study, the general flow regimes and macroscopic flow structures of a three-phase fluidized bed are similar to those of a bubble column although the size of the flow structure may deviate. The deviation is due to the change in the apparent rheological properties of the mixture and the extra interphase interactions caused by the solid particles. Under the same gas and liquid velocities, the solids phase does not significantly affect the transition of the flow regimes. This finding which is based on the flow visualization with water as the liquid phase and solids holdup below 10%, however, may not be applicable for the flow with high solids holdups. The sodium iodide solution used as the liquid phase for the refractive index matching of the glass beads introduces the liquid property effects, such as viscosity effect and surfactant effect, on the flow structure of the three-phase fluidization. The study of these effects is beyond the intent of this work.

The flow structure of the liquid phase in the vortical-spiral flow regime of a three-phase fluidized bed is shown in Figure 14, specifically the liquid flow pattern at the plane of 0.75 radius for three-phase fluidization with solids holdup of 5% under liquid-batch condition and a gas velocity of 2.9 cm/s. Due to the refractive index matching, the solids phase becomes "invisible" in the figure. Similar vortical and spiral flow pattern as in a bubble column is observed. The solids flow pattern can be detected by slightly mismatching the refractive index between the solids and liquid phases. It should be noted that a slight mismatch of the refractive index between the liquid and solids phases restricts the observation of the flow structure to below 10% solids holdup condition. Through the flow visualization and PIV results, the flow pattern of the solids phase is found to be similar to the liquid phase with negligible velocity lag between the 500 μm glass bead particles and the sodium iodide liquid.

Concluding Remarks

Macroscopic flow structures in 3-D bubble columns and gas-liquid-solid fluidization systems are investigated through flow visualization using laser sheeting. Particle image velocimetry is used for quantification of the flow structures. The PIV system provides full-field, instantaneous flow information which is crucial to further understanding the dynamic nature of fluidization systems. Three flow regimes are identified which vary with the gas and liquid velocities. Under low gas flow velocities and high liquid velocities, the dispersed bubble re-

gime prevails as the bubbles rise rectilinearly and the liquid/solids phase falls downward between the bubble streams. Further increase in gas velocity results in the transition of flow regime into the vortical-spiral flow regime. In the vortical-spiral flow regime, clusters of bubbles or coalesced bubbles form the central bubble stream moving in a spiral manner with the liquid/solids phase not only moving in a vortical pattern but also spiraling downward in the region between central bubble stream and the column wall. Four flow regions—descending flow region, vortical-spiral flow region, fast bubble flow region, and central plume region—are identified in the vortical-spiral flow regime. The four flow regions are instantaneous phenomena which deviate from the flow characteristics obtained when time averaging procedures are used to quantify the flow properties. The bubble coalescence becomes dominant and forms large bubbles as the flow regime moves into the turbulent flow regime at high gas velocities. Local chaotic motion of the liquid/solids phase, caused by the bubble wake and drift effects due to the bubble motion, progressively destroys the vortical and spiral flow structure and leads to the turbulent flow structure. The increase of liquid velocity affects the transition of the flow regimes and the size of the flow structure. However, the existence of the solids phase under low solids holdups does not exhibit significant effects on either the transition of the flow regime or the size of the flow structure. The transition of the flow regimes and the flow structure in the vortical-spiral flow region are found to be analogous to the Taylor stability postulation and its resulted turbulent vortices structure for the flow between two concentric rotating cylinders. Similarities between the flow structure of two-dimensional and three-dimensional systems are also identified.

Acknowledgment

The work was supported by the National Science Foundation Grant CTS-9200793.

Notation

a = inner cylinder radius
b = outer cylinder radius
Re_d = Reynolds number
R_i = inner cylinder Reynolds number
R_o = outer cylinder Reynolds number
T_a = Taylor number
U_g = gas velocity
U_i = peripheral velocity of the inner cylinder
U_l = liquid velocity

Greek letters

ϵ_s = solids holdup
ν = liquid kinematic viscosity
ρ_s = particle density
Ω_i = angular velocity of the inner cylinder
Ω_o = angular velocity of the outer cylinder

Literature Cited

Andereck, C. D., S. S. Liu, and H. L. Swinney, "Flow Regimes in a Circular Couette System with Independent Rotating Cylinders," *J. Fluid Mech.*, **164**, 155 (1986).

Anderson, K. G., and R. G. Rice, "Local Turbulence Model for Predicting Circulation Rates in Bubble Columns," *AIChE J.*, **35**, 514 (1989).

Bhavaraju, S. M., T. W. F. Russell, and H. W. Blanch, "The Design of Gas Sparged Devices for Viscous Liquid Systems," *AIChE J.*, **24**, 454 (1978).

Chen, R. C., and L.-S. Fan, "Particle Image Velocimetry for Characterizing the Flow Structure in Three-Dimensional Gas-Liquid-Solid Fluidized Beds," *Chem. Eng. Sci.*, **47**, 3615 (1992).

Clark, N. N., C. M. Atkinson, and R. L. C. Flemmer, "Turbulent Circulation in Bubble Columns," *AIChE J.*, **33**, 515 (1987).

Couette, M., "Etudes sur le Frottement des Liquides," *Ann. Chim. Phys.*, **21**, 433 (1890).

Deckwer, W.-D., Y. Louisi, A. Zaidi, and M. Ralek, "Hydrodynamic Properties of the Fischer-Tropsch Slurry Process," *I&EC Process Des. & Dev.*, **19**, 699 (1980).

Devanathan, N., D. Moslemian, and M. P. Dudukovic, "Flow Mapping in Bubble Columns Using CARPT," *Chem. Eng. Sci.*, **45**, 2285 (1990).

Drahoš, J., J. Zahradník, M. Fialová, and F. Bradka, "Identification and Modelling of Liquid Flow Structure in Bubble Column Reactors," *Int. Conf. on Gas-Liquid and Gas-Liquid-Solid Reactor Engineering*, Columbus, OH (Sept. 13-16, 1992).

Drazin, P. G., and W. H. Reid, *Hydrodynamic Stability*, Cambridge University Press (1981).

Fan, L.-S., K. Muroyama, and S. H. Chern, "Hydrodynamic Characteristics of Inverse Fluidization in Liquid-Solid and Gas-Liquid-Solid Systems," *Chem. Eng. J.*, **24**, 143 (1982).

Fan, L.-S., *Gas-Liquid-Solid Fluidization Engineering*, Butterworth, Stoneham, MA (1989).

Fan, L.-S., and K. Tsuchiya, *Bubble Wake Dynamics in Liquids and Liquid-Solid Suspensions*, Butterworth, Stoneham, MA (1990).

Fiebig, M., and N. K. Mitra, eds., *Vortices and Heat Transfer, Proc. of the Seminar, Eurotherm 31*, Ruhr-Universität Bochum, Germany (May 24-26, 1993).

Franz, K., T. Borner, H. J. Kantorek, and R. Buchholz, "Flow Structures in Bubble Columns," *Ger. Chem. Eng.*, **7**, 365 (1984).

Geary, N. W., and R. G. Rice, "Circulation and Scale-Up in Bubble Columns," *AIChE J.*, **38**, 76 (1992).

Hills, J. H., "Radial Non-Uniformity of Velocity and Voidage in a Bubble Column," *Trans. IChemE*, **52**, 1 (1974).

Joshi, J. B., and M. M. Sharma, "A Circulation Cell Model for Bubble Columns," *Trans. IChemE*, **57**, 244 (1979).

Joshi, J. B., "Axial Mixing in Multiphase Contactors—A Unified Correlation," *Trans. IChemE*, **58**, 155 (1980).

Kaye, J., and E. C. Elgar, "Modes of Adiabatic and Diabatic Fluid Flow in an Annulus with Inner Rotating Cylinder," *Trans. ASME*, **80**, 753 (1958).

Latif, B. A. J., and J. F. Richardson, "Circulation Patterns and Velocity Distributions for Particles in a Liquid Fluidised Bed," *Chem. Eng. Sci.*, **27**, 1933 (1972).

Lin, J. S., M. M. Chen, and B. T. Chao, "A Novel Radioactive Particle Tracking Facility for Measurement of Solids Motion in Gas Fluidized Beds," *AIChE J.*, **31**, 465 (1985).

Ludwieg, H., "Experimentelle Nachprüfung der Stabilitätstheorien für reibungsfreie Strömungen mit schraubenlinienförmigen Stromlinien," *Z. Flugwiss*, **12**, 304 (1964).

Reese, J., R. C. Chen, J.-W. Tzeng, and L.-S. Fan, "Characterization of the Macroscopic Flow Structure in Gas-Liquid and Gas-Liquid-Solid Fluidization Systems Using Particle Image Velocimetry," video presentation, *Int. Conf. Gas-Liquid and Gas-Liquid-Solid Reactor Engineering*, Columbus, OH (Sept. 13-16, 1992); *Int. Video J. Eng. Res.*, in press (1994).

Rietema, K., and Ir. S. P. P. Ottengraf, "Laminar Liquid Circulation and Bubble Street Formation in a Gas-Liquid System," *Trans. IChemE*, **48**, T54 (1970).

Rice, R. G., and M. Littlefield, "Dispersion Coefficients for Ideal Bubbly Flow in Truly Vertical Bubble Columns," *Chem. Eng. Sci.*, **42**, 2045 (1987).

Rice, R. G., and N. W. Geary, "Prediction of Liquid Circulation in Viscous Bubble Columns," *AIChE J.*, **36**, 1339 (1990).

Rice, R. G., D. T. Barbe, and N. W. Geary, "Correlation of Non-Verticality and Entrance Effects in Bubble Columns," *AIChE J.*, **36**, 1421 (1990).

Rice, R. G., N. W. Geary, and L. F. Burns, "Circulation Model for

Absorption and Dispersion in Cocurrent Bubble Columns," *AIChE J.*, **39**, 224 (1993).
Schlichting, H., *Boundary-Layer Theory*, McGraw-Hill, New York (1979).
Tang, W.-T., and L.-S. Fan, "Hydrodynamics of a Three-Phase Fluidized Bed Containing Low-Density Particles," *AIChE J.*, **35**, 355 (1989).
Taylor, G. I., "Stability of a Viscous Liquid Contained between Two Rotating Cylinders," *Phil. Trans.*, **A223**, 289 (1923).
Ting, J. T., and A. A. H. Drinkenburg, "The Influence of Slight Departures from Vertical Alignment of Liquid Dispersion and Gas Hold-up in a Bubble Column," *Chem. Eng. Sci.*, **41**, 165 (1986).
Tsuchiya, K., G.-H. Song, W.-T. Tang, and L.-S. Fan, "Particle Drift Induced by a Rising Bubble in a Liquid-Solid Fluidized Bed Containing Low-Density Particles," *AIChE J.*, **38**, 1847 (1992).
Tzeng, J.-W., R. C. Chen, and L.-S. Fan, "Visualization of Flow Characteristics in a 2-D Bubble Column and Three-Phase Fluidized Bed," *AIChE J.*, **39**, 733 (1993).
Ueyama, K., and T. Miyauchi, "Properties of Recirculating Turbulent Two Phase Flow in Gas Bubble Columns," *AIChE J.*, **25**, 258 (1979).
Ulbrecht, J. J., Y. Kawase, and K. F. Auyeung, "More on Mixing of Viscous Liquids in Bubble Columns," *Chem. Eng. Commun.*, **35**, 175 (1985).
Walter, J. F., and H. W. Blanch, "Liquid Circulation Patterns and Their Effect on Gas Hold-Up and Axial Mixing in Bubble Columns," *Chem. Eng. Commun.*, **19**, 243 (1983).
Whalley, P. B., and J. F. Davidson, *Inst. Chem. E./Inst. Mech. E. Symp. on Multi-Phase Flow Systems*, Ser. No. 38, 55 (1974).

Manuscript received May 21, 1993, and revision received Sept. 30, 1993.